

Flat-Foldable Rigid Origami with Uniform-Thickness Panels

Yuta Shimoda^{1,*}, Tomohiro Tachi^{2,*}, Jun Sato¹

¹ Graduate School of Frontier Sciences, The University of Tokyo, Chiba, Japan

² Graduate School of Arts and Sciences, The University of Tokyo, Tokyo, Japan

* Corresponding authors e-mail: simo4mo314@gmail.com, tachi@idea.c.u-tokyo.ac.jp

Abstract

In this paper, we present a novel design method of rigidly foldable origami composed of panels with uniform thicknesses. Our design is based on quadrilateral-transformable mesh composed of degree-4 vertex with equal opposite sector angles, forming a family of corrugated surfaces that folds flat. We apply thickness to such a rigidly foldable surface by extending the axis-shift method to degree-4 vertex with equal opposite angles. Using our method, each panel ends up having uniform thickness.

We investigate the necessary and sufficient conditions on the pair of opposite angles and the thickness ratio for each saddle-like vertex to maintain the kinematics after thicknesses were applied. We construct parametric design models based on the derived constraints and explore the design space. The design examples of transformable structures are potentially applicable to architectural design. The resulting structures efficiently fold up to completely flat states with 180° fold angles, wherein the total thickness is the sum of the thicknesses of overlapping panels. This also allows for fabrication by first cutting out each panel and subsequently assembling them in the flat-folded state.

Keywords: origami, thick rigid origami, spatial linkage, discrete Voss surface

1 Introduction

Rigid origami, which is the origami model composed of rigid panels and hinges, is useful for various engineering purposes, especially for designs of transformable architecture. Although origami models are mathematically considered to have a zero-thickness surface, this is no longer true when applied to physical mechanisms. Especially, in the design of architectural space, we need structures composed of thick panels or composite three-dimensional structure with a finite volume to bear gravity and other loads as well as to insulate against heat, radiation, sound, among others. Adding thickness can alter the kinematics of the rigid origami; therefore, several approaches are proposed to achieve thick rigid origami (Lang et al. 2018; Hoberman 1988; Tachi 2011; Chen et al. 2015). There are two major approaches. Tachi (2011) proposed an approach based on trimming panel volumes, i.e., the panel offset and the panel tapering as shown in [fig. 1](#) middle and right. This approach is universal in the sense that the original kinematics of rigid origami is maintained. However, obtaining a completely flat-folded state is not possible as the volume starts to block the folds.

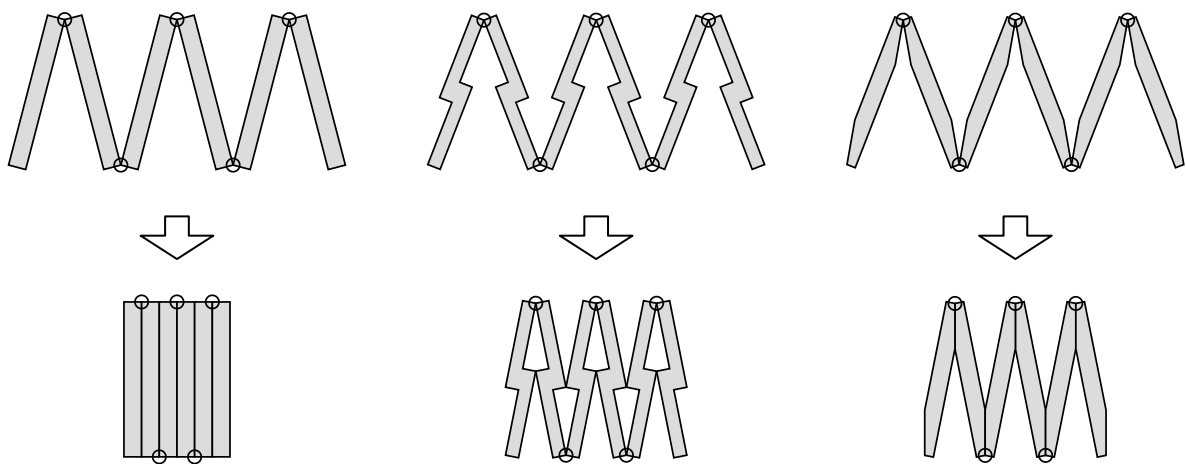


Figure 1: Three approaches for enabling thick panel origami. Left: panels with uniform thickness using the axis-shift approach, which folds completely flat compared to the volume trim method by Tachi (2011) (Middle: with panel offset; and Right: with panel tapering).

The other is an approach based on the shifting rotation axis as shown in [fig. 1](#) left. Shifted axes change the kinematics of rigid origami from a spherical linkage to a spatial linkage, so the method applies to limited types of vertices satisfying conditions between thicknesses and the sector angles. Hoberman (1988) first proposed the thickness method of rigid origami using axis-shift applied to mirror-symmetric Miura-ori vertices. The method allows for obtaining various rigidly foldable structures with thick panels (Hoberman 2010). Chen et al. (2015) extended the axis-shift method to non-mirror-symmetric flat-foldable developable degree-4 vertices. Structures created using axis-shift approach can fold to a complete flat folding of 180° without any interference.

The focus of existing approaches of thick rigid origami was limited to developable origami surfaces. However, for architectural applications, the developability of the entire surface is not necessarily required because the assembly of multiple parts is necessary due to the available size of the panel materials. Instead, we can explore wider variety of deployable structures from families of non-developable but flat-foldable rigid origami. Our objective is to propose a fabrication-aware method of thick panel construction for non-developable but flat-foldable rigid origami.

In this paper, we propose a family of flat-foldable origami composed of thick panels by extending the axis-shift approach to a mesh composed of degree-4 vertex with equal opposite sector angles. Such surfaces are known as discrete Voss surfaces as their smooth version corresponds to Voss-net, i.e., conjugate geodesic net, and are rigidly foldable as shown in Schief et al. (2008); Tachi (2010). The surfaces are not necessarily developable but have one-degree of freedom (DOF) mechanism that folds flat.

In our method, each panel ends up having uniform thickness, it is planar. There is no unevenness, and the thickness is even for each panel. This is a novel property, and the resulting structures efficiently fold up to completely flat states with 180° fold angles, wherein the total thickness is the sum of the thicknesses of overlapping panels. This also allows for fabrication by first cutting out each panel and subsequently assembling them in the flat-folded state.

In [sec. 2](#), we first review the kinematics of discrete Voss surfaces with zero thickness, and the condition for the sector angles to make it rigidly foldable. Then, we demonstrate methods for constructing thickness that maintains the kinematics in [sec. 3](#), and formulate the conditions between the sector angles and the thickness. Based on the conditions, we explore design space in [sec. 4](#) to show freeform examples and symmetric shapes.

2 Discrete Voss Surfaces with Zero Thickness

Discrete Voss surfaces are the discretised version of conjugate geodesic nets, i.e., a quadrivalent mesh where each face is planar, and the opposite angles are equal at each vertex ([fig. 2](#)) (Schief et al. 2008). We consider the family of discrete Voss surfaces with corrugation, i.e., the mountain and valley creases are alternately repeated. When the surface is corrugated in both the row and column directions, we obtain the generalization of eggbox surfaces, often bidirectionally flat-foldable without self-intersection ([fig. 3](#)). Similarly, when the surfaces are corrugated only in the row direction, we obtain surfaces that are often one-way flat-foldable without an intersection.

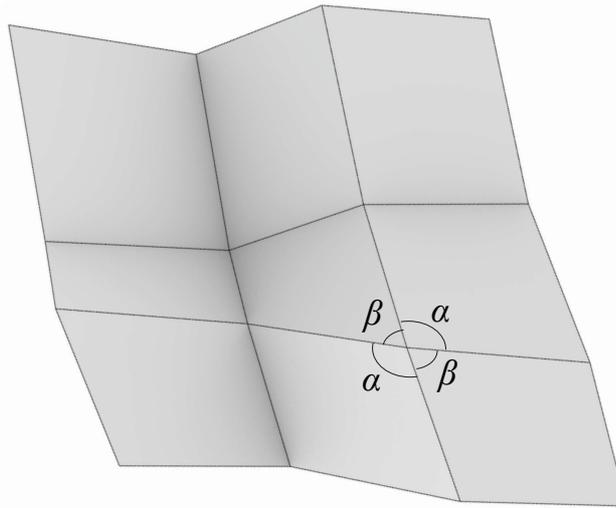


Figure 2: Definition of discrete Voss surface.

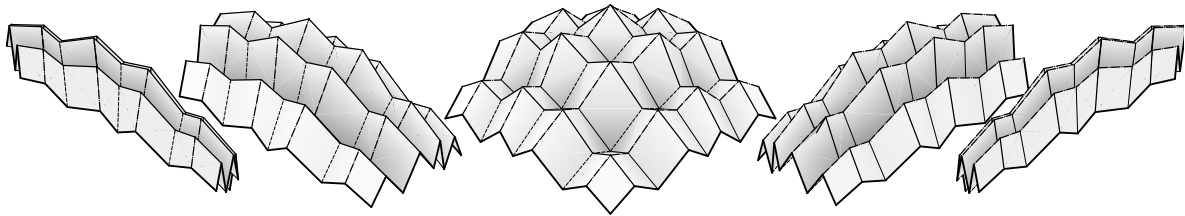


Figure 3: Folding motion of a generalized eggbox surfaces.

Each vertex has four rotation axes meeting at a point and thus forms a spherical 4R mechanism of one-DOF. In general, connecting these vertices into a mesh creates an over-constrained system and is not guaranteed to form a mechanism. The rigid foldability of discrete Voss surfaces is proved by Schief et al. (2008). More precisely, the existence of an intermediate folded state (a folded state not in a plane) guarantees the existence of a mechanism (Tachi 2010), whereas the direct construction of such a folded state often requires numerical computation using optimization algorithms. In this study, we introduce an alternative approach using an analytical loop condition to guarantee the folding motion of structures parameterized only by intrinsic parameters, i.e., the sector angles of panels, instead of directly computing the folded state embedded three-dimensionally.

Herein, we state that the kinematics of vertices with equal opposite angle whose sector angles are $\alpha, \beta, \alpha, \beta$ in counterclockwise order is equivalent to that of flat-foldable developable degree-4 vertex with sector angles $\alpha, \beta, \pi - \alpha, \pi - \beta$ as shown in [fig. 4](#). Specifically, the fold angle of one opposing pair in the Miura-ori is equal to the supplementary fold angle in the discrete Voss surface. We adapt the rigid-foldability condition of developable flat-foldable origami (Tachi and Hull 2017)

to obtain the one for discrete Voss surfaces. By adapting Tachi and Hull (2017) to the supplementary fold angles, for each vertex with sector angles $\alpha, \beta, \alpha, \beta$, we obtain the fold angles provided by $\rho_x, \rho_y, \rho_x, \rho_y$, which are related as

$$\tan \frac{\rho_x}{2} \tan \frac{\rho_y}{2} = p(\alpha, \beta), \tag{1}$$

where

$$p(\alpha, \beta) := \frac{1 - \tan \frac{\alpha}{2} \tan \frac{\beta}{2}}{1 + \tan \frac{\alpha}{2} \tan \frac{\beta}{2}}. \tag{2}$$

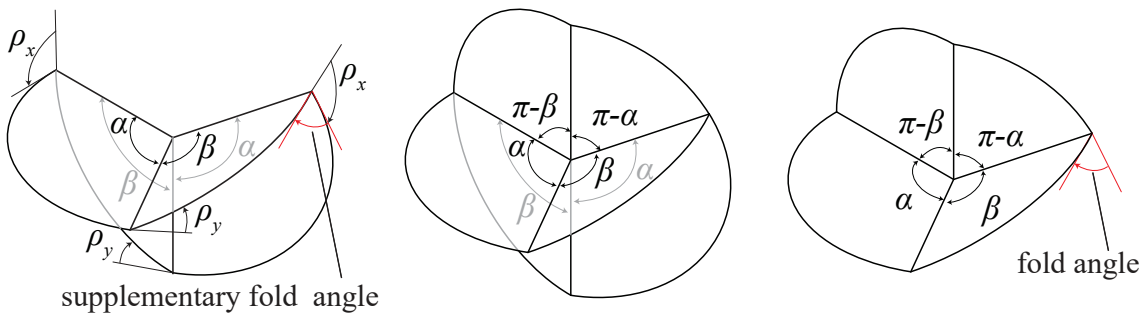


Figure 4: Left: a vertex of discrete Voss surface whose sector angles are $\alpha, \beta, \alpha, \beta$. Right: a vertex of Miura-ori whose sector angles are $\alpha, \beta, \pi - \alpha, \pi - \beta$. The set of planes used is identical (Middle), and the supplementary angle of the discrete Voss vertex is equal to the fold angle of the Miura-ori vertex.

In this mechanism, we always have two opposing pairs of creases of equal fold angles, i.e., ρ_x or ρ_y , where one of them approaches 180° when the other reaches 0° , i.e., when an opposite pair of creases fold, the other pair unfolds. In general, the kinematics has two branching modes of one-DOF mechanisms; however, we already excluded the other mode represented by $\rho_x, \rho_y, -\rho_x, -\rho_y$ (with different speed coefficient) because the mode always produces self intersection.

Now, we consider a cycle around each *interior* quadrangle, i.e., a face not incident to vertices on the boundary, as shown in **fig. 5**; they are surrounded by creases $i = 0, \dots, 3 \pmod 4$ with fold angles ρ_i . For each corner formed by sector angles $\alpha_{i,i+1}, \beta_{i,i+1}, \alpha_{i,i+1}, \beta_{i,i+1}$, the relation of fold angles is given by:

$$\tan \frac{\rho_i}{2} \tan \frac{\rho_{i+1}}{2} = p_{i,i+1}, \tag{3}$$

where $p_{i,i+1} := p(\alpha_{i,i+1}, \beta_{i,i+1})$. This equation sequentially relates the fold angles of adjacent creases around the quadrangle, which then needs to be consistent when it cycles back. For the neighborhood of the interior quadrangle to be consistently

rigidly foldable, it is necessary and sufficient to satisfy the following:

$$\frac{p_{01}p_{23}}{p_{12}p_{30}} = 1. \quad (4)$$

For the entire mesh to be rigidly foldable (ignoring global self-intersection), it is necessary and sufficient to satisfy [eq. \(4\)](#) for each interior quadrangle.

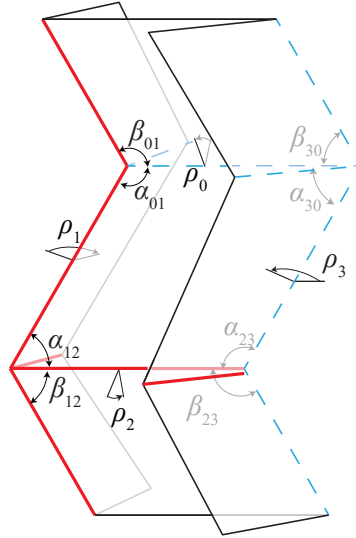


Figure 5: Sector angles and fold angles of the interior face of a discrete Voss surface.

3 Degree-4 Vertex with Uniform Thickness

3.1 Single Vertex

For thickness accommodation based on the axis-shift method, we first classify the vertices based on the mountain-and-valley (MV) assignment of the opposing pairs because the axis needs to lie on the valley side of the thick panels. From [eq. \(2\)](#), we can observe that when $\alpha + \beta \in (0, \pi)$, $p(\alpha, \beta) > 0$ and thus the MV-assignment for all creases are the same; subsequently, when $\alpha + \beta \in (\pi, 2\pi)$, $p(\alpha, \beta) < 0$ and thus the MV-assignment of opposite pairs are opposite. We call the former a saddle-like vertex and the latter a convex vertex. Developable vertices with $\alpha + \beta = 180^\circ$ can fold in both assignments, so either type can be applied as shown in [sec. 3.1](#). The necessary and sufficient conditions on the convex vertices and saddle vertices are summarized below.

Convex Case

When adding thickness to convex vertices, we can add the thickness on the convex side of the vertex to ensure that all fold lines still intersect at one point ([fig. 6](#)). In this case, the mechanism is still a spherical 4R mechanism, and thus transformable regardless of the thickness.

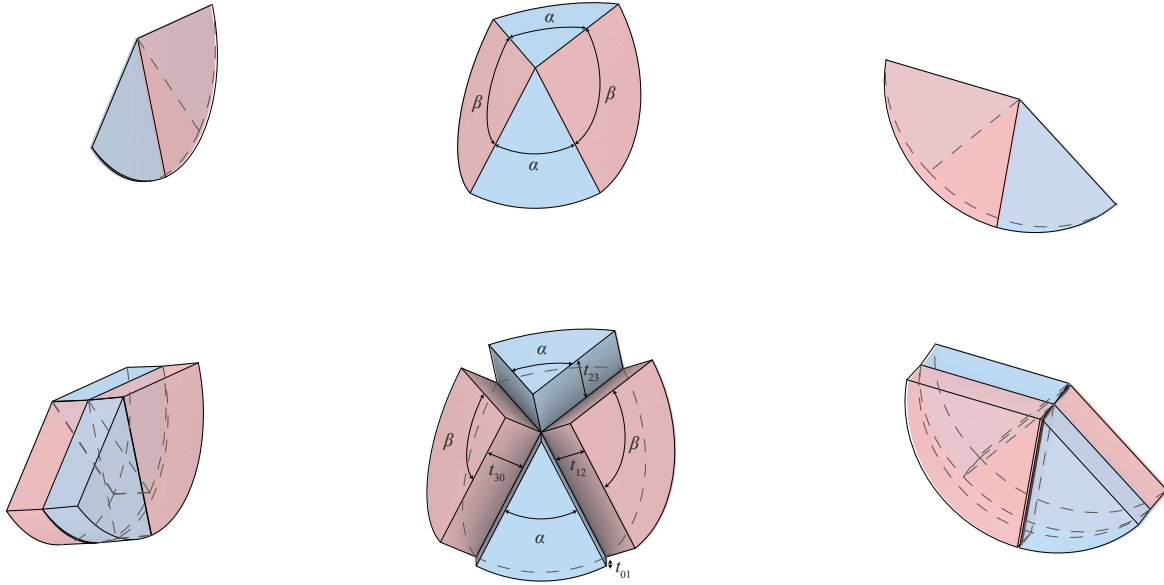


Figure 6: Folding motion of a convex vertex (a vertex with positive Gaussian curvature). Top: with zero thickness. Bottom: with uniform thickness.

Saddle-Like Case

When adding thickness to saddle-like vertices, an opposite pair of axes with mountain creases shift inward, and the other opposite pair with valley creases shift outward. This forms a spatial 4R linkage (**fig. 7**), which is not generally a mechanism; Bennett linkage (Bennett 1903) is the only known spatial 4R linkage. Chen et al. (2015) applied Bennett linkage to the thickness method for developable degree-4 Miura-ori vertices. We can similarly construct a Bennett linkage in our case by carefully choosing the thickness of panels $t_{i,i+1}$ (between creases i and $i+1$) that corresponds to the length of bars in the linkage. Therefore, we obtain the following constraints.

$$t_{01} = t_{23}, t_{12} = t_{30}. \quad (5)$$

$$\frac{t_{12}}{t_{01}} = \frac{\sin \beta}{\sin \alpha}. \quad (6)$$

Developable Case

When the vertices are developable, i.e., $\alpha + \beta = 180^\circ$, both convex and saddle-like types can be applied, as shown in **fig. 8**. When the convex-type thickness is chosen, the opposing pairs have both mountains, while when the saddle-like type is chosen, the opposing pairs have a mountain and a valley. If the saddle-like construction is chosen, the thickness of both panels needs to be the same because $\sin(\alpha) = \sin(\pi - \alpha)$. The folding motion of the vertex is singular: an opposing pair stays unfolded while the other pair continuously fold. These transforming and non-transforming pairs switch in the developed state.

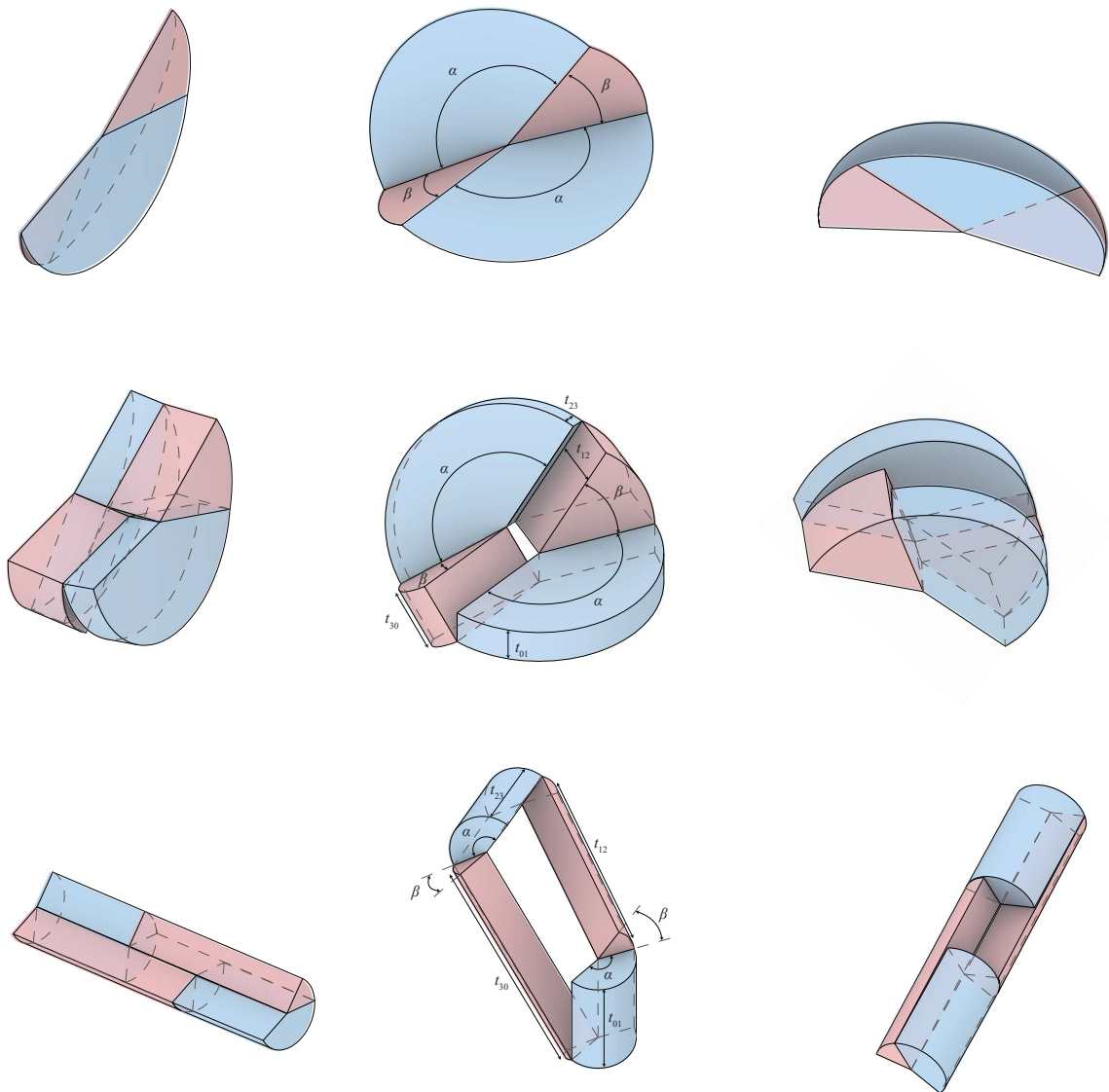


Figure 7: Folding motion of a saddle-like vertex (a vertex with negative Gaussian curvature) with zero thickness (top) and with uniform thickness (middle), and corresponding Bennett linkage (bottom).

3.2 Combined Geometric Conditions

We set the design parameters as the sector angles at each corner and the thicknesses of panels. Based on the above constraint conditions, necessary and sufficient conditions for a rigidly foldable structure with uniform panels can be obtained. The rigid foldability (and existence) conditions for the zero-thickness discrete Voss surfaces are as follows.

- The opposite sector angles at each vertex are equal.
- For each interior face, the sum of its sector angles is 360° .

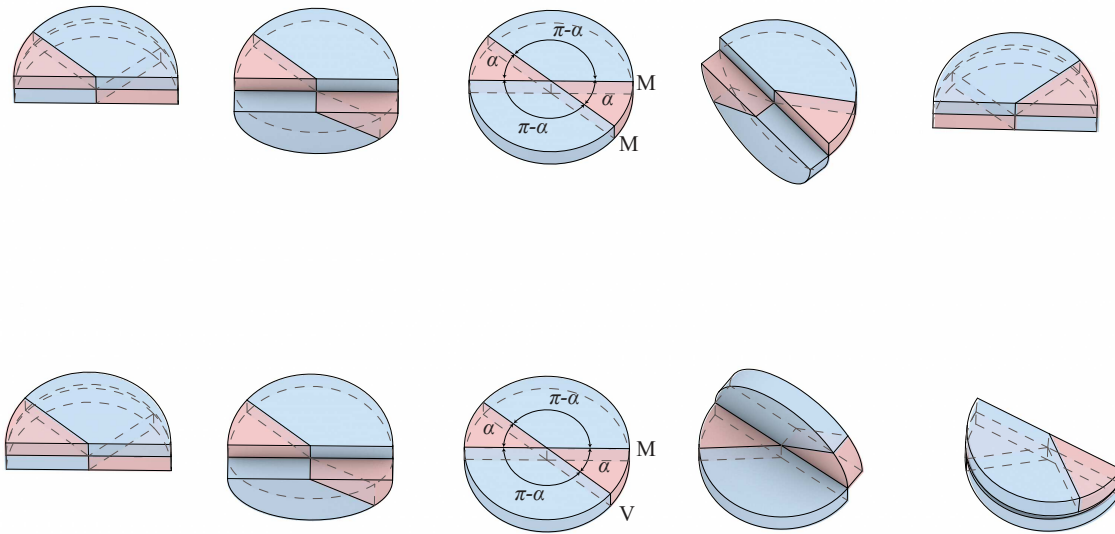


Figure 8: Folding motion of developable vertices with different thickness types. Top: the convex construction allows for the folding motion with four creases with same assignment. Bottom: the saddle-like construction allows the opposing pairs to have opposite MV-assignment.

- For each interior face, the sector angles satisfy the loop constraint given by [eq. \(4\)](#).

For accommodation of thickness, we add a condition as follows.

- The sector angles and thicknesses satisfy [eq. \(5\)](#) and [eq. \(6\)](#) at each saddle-like vertex.

When all these conditions are met, we obtain rigidly foldable discrete Voss surfaces with thickness. The DOF of design, i.e., the number of independent parameters we can choose can vary based on the numbers of panels and saddle-like vertices. In some cases, we may want to restrict the thicknesses to that of commercially available materials with standard dimensions; in this case, we expect a smaller number of DOF of design. We investigate the DOF of design and the design examples in the following section.

4 DOF of Design

We consider the DOF of design of the mesh with $n \times m$ quadrangle panels, which has $(n-1)(m-1)$ interior vertices and $(n-2)(m-2)$ interior panels. According to [sec. 3.2](#), the DOF of design of the surface with zero thickness is observed by subtracting the number of constraints from the number of sector angles of all interior vertices, i.e.

$$4(n-1)(m-1) - (2(n-1)(m-1) - 2(n-2)(m-2)) = 2n + 2m - 6. \quad (7)$$

If the number of types of thicknesses applied to panels connected to saddle-like vertices is denoted by T and the number of saddle-like vertices is denoted by S , then the DOF of design is $2n + 2m + T - S - 7$. Especially, when $T = 1$, i.e., the surface is composed of panels with a single type of thickness, the DOF of design is $2n + 2m - S - 6$.

The numbers T and S can vary by the MV-assignment on the creases, i.e., how the surface is corrugated. Here, we pick up two typical types: the eggbox type –when the surface is corrugated in both row and column directions– and the bellows type –when the surface is corrugated only in column direction and has same convexity in the perpendicular direction–. The eggbox-type surface is often bidirectionally flat-foldable without self-intersection, as shown in [fig. 10](#). The bellows-type surface is often one-directionally flat-foldable without intersection, as shown in [fig. 12](#). Here, for the simplicity of discussion, we assume that n and m are odd numbers; therefore, the number of mountain and valley creases are equal.

4.1 Eggbox-type

In an eggbox-type surface, the number of saddle-like vertices is $\frac{1}{2}(n-1)(m-1)$ ([fig. 10](#) Top row). Moreover, the maximum number of different thicknesses that can be applied is $n + m - 3$ because for each saddle-like vertex, the opposing panels must have the same thickness. The DOF of design for the structures with zero thickness, multiple types of thicknesses, and single type of thickness is shown in [tab. 1](#) and [fig. 10](#) middle row. An example design of eggbox-type structure of 3×3 panels is shown in [fig. 10](#) bottom row. The structure folds to a completely flat state to column (resp., row) directions, when the total thickness is the sum of thicknesses along the columns (resp., rows).

Zero Thickness	Multiple Thicknesses	Single Thickness
$2n + 2m - 6$	$14 - \frac{(n-7)(m-7)}{2}$	$6 - \frac{(n-5)(m-5)}{2}$

Table 1: DOF of design of eggbox-type surface with $n \times m$ panels.

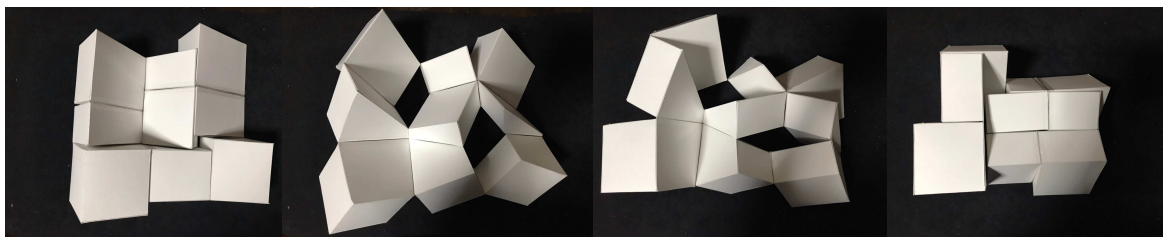


Figure 9: Folding motion of an eggbox-type model composed of 3×3 panels to which three types of thicknesses are applied.

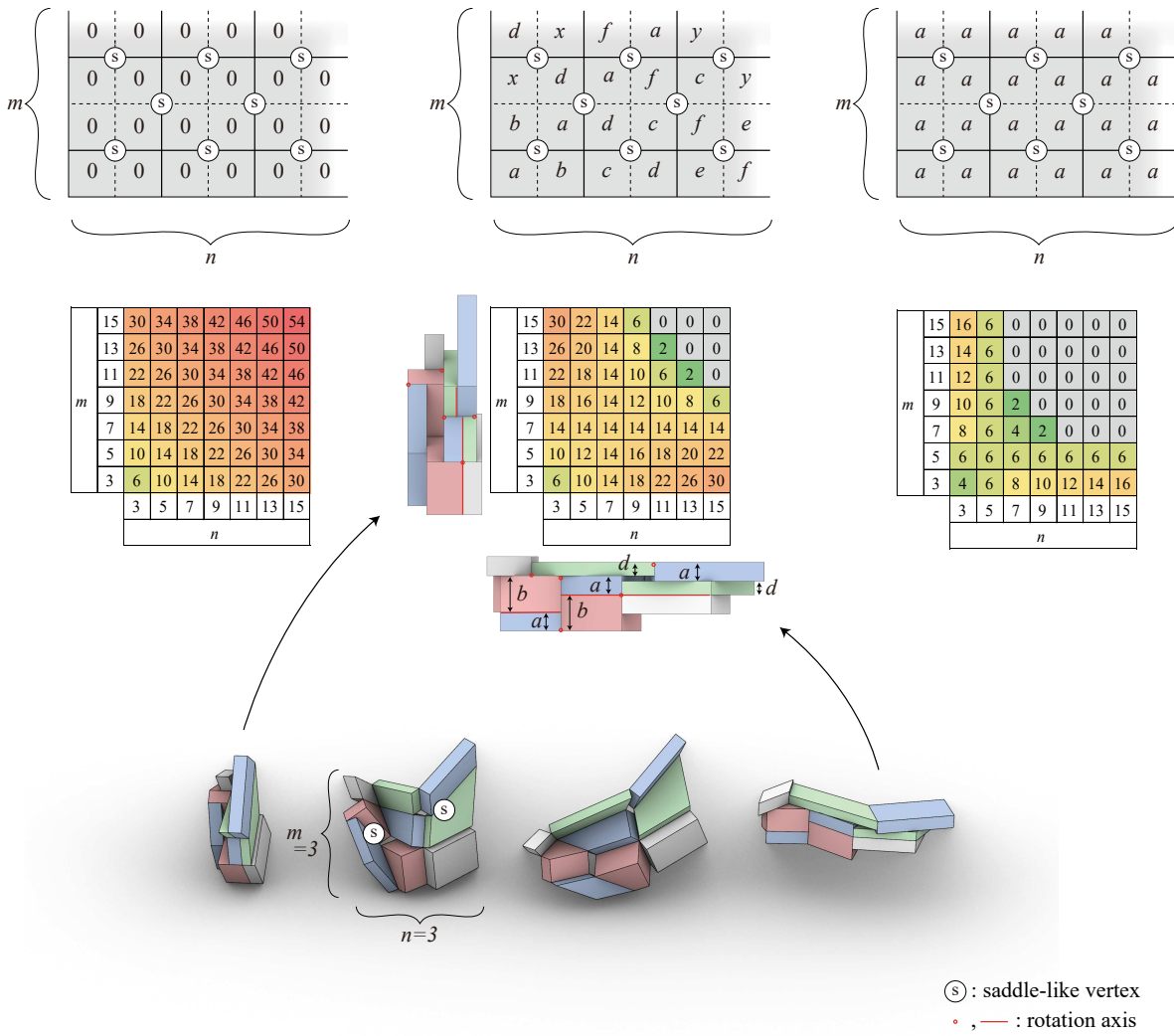


Figure 10: Top row: the saddle vertices (marked as S) and thickness assignment in eggbox-type surfaces composed of $n \times m$ panels with zero thickness (left), multiple thicknesses (middle), and single thickness (right). Middle row: the tables of the DOF of design computed from **tab. 1** for n, m between 3 and 15, with zero thickness (left), multiple thicknesses (middle), and single thickness (right). Bottom row: the folding motion of an example eggbox-type surface 3×3 panels.

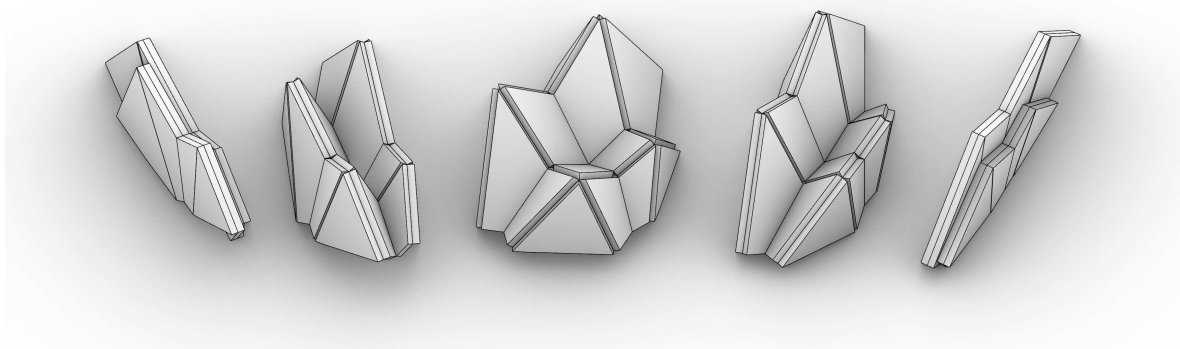


Figure 11: Folding motion of a freeform eggbox-type structure composed of 4×4 panels using 4 types of thicknesses.

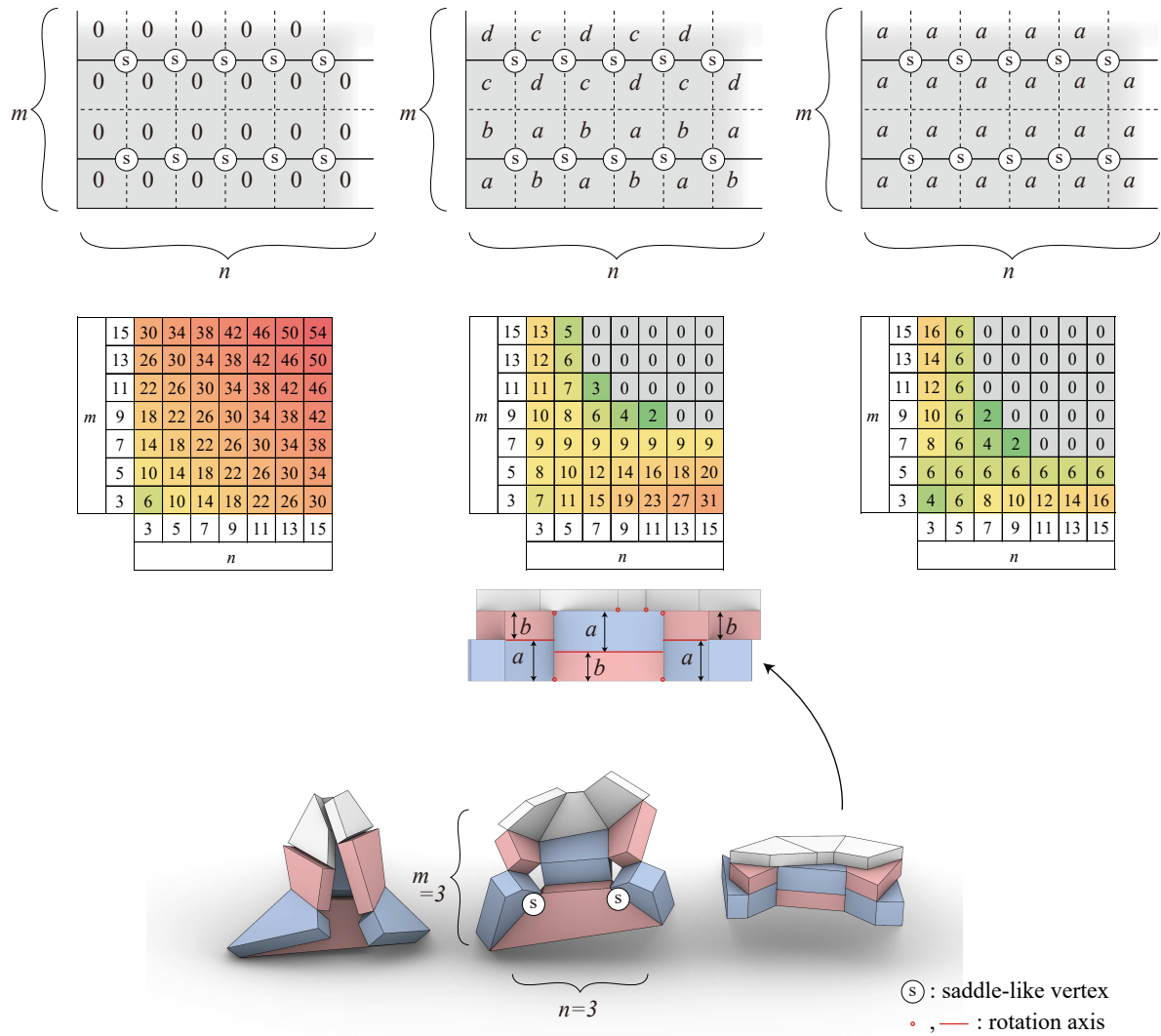


Figure 12: Top row: the saddle vertices (marked as S) and thickness assignment in bellows-type surfaces composed of $n \times m$ panels with zero thickness (left), multiple thicknesses (middle), and single thickness (right). Middle row: the tables of the DOF of design computed from **tab. 2** for n, m between 3 and 15, with zero thickness (left), multiple thicknesses (middle), and single thickness (right). Bottom row: the folding motion of an example bellows-type surface 3×3 panels.

4.2 Bellows-type

In a bellows-type surface, the number of saddle-like vertices is $\frac{1}{2}(n-1)(m-1)$ and the maximum number of different thicknesses that can be applied is $m-1$ (**fig. 12** Top row) The DOF of design of the surfaces with zero thickness, multiple types of thicknesses, and single thickness are shown in **tab. 2** and **fig. 12** middle row. An example design of a bellows-type structure of 3×3 panels is shown in **fig. 12** bottom row. The structure folds to a completely flat state in the column direction when the total thickness is the sum of thicknesses along the columns.



Figure 13: Folding motion of a freeform bellow-type structure composed of 4×4 panels using 2 types of thicknesses.

Zero Thickness	Multiple Thicknesses	Single Thickness
$2n + 2m - 6$	$9 - \frac{(n-7)(m-5)}{2}$	$6 - \frac{(n-5)(m-5)}{2}$

Table 2: DOF of design of a bellows-type surface with $n \times m$ panels.

4.3 Characterization

As shown in **tab. 1** and **tab. 2**, the DOF of design is provided by a quadratic form of m and n . More specifically, we obtain the hyperbolic form of $k - (n - n_0)(m - m_0)$ with asymptotic lines of $n = n_0$ and $m = m_0$. This suggests that if $n \leq n_0$ (or $m \leq m_0$, resp.), we can increase m (or n , resp.) arbitrarily while we still have design freedom. However, when both n and m increase, the DOF becomes negative, i.e., the structure is over-constrained, unless the constraints are degenerate. Therefore, for a larger n and m , it is reasonable to find the design method assuming certain symmetry to make the constraints degenerate, as shown in the subsequent examples.

5 Design from Symmetry

5.1 Generating from Polyline

We demonstrate a design approach to create an cylindrical vault shape from a given arbitrary section polyline. The resulting structure is composed of panels of single type of thickness, and folds flat to its longitudinal direction.

We first consider a planar polyline $P_0P_1P_2 \dots P_n$ on xz -plane (**fig. 14**), which can be any simple planar polyline with possible concavity or corrugation. We extend this polyline toward the y direction to construct a vault surface that folds flat in the y direction.

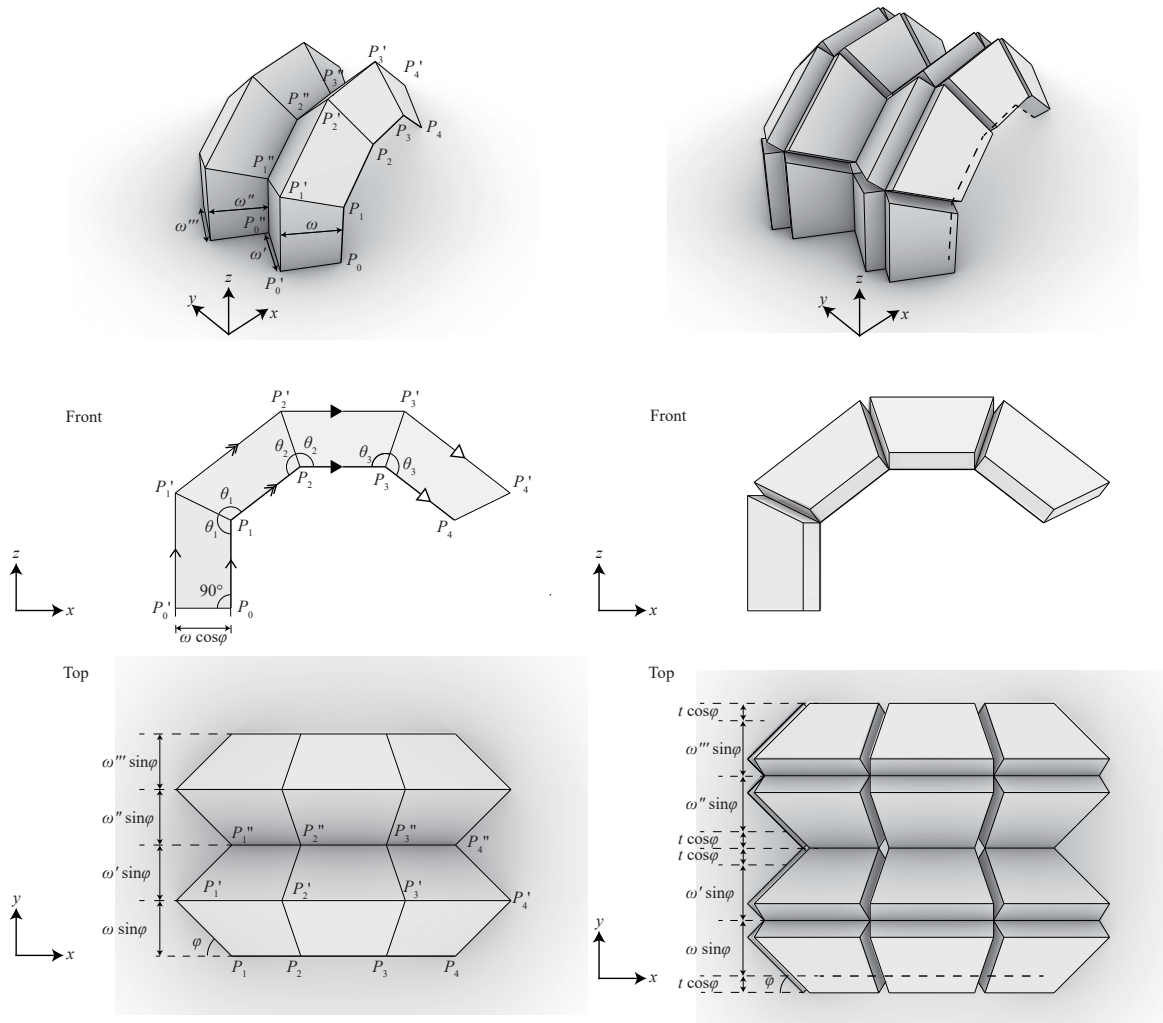


Figure 14: One-way flat-foldable mechanism wherein mountain and valley creases are alternately repeated only in one direction. Left: zero thickness. Right: every panel with equal thickness.

The procedure to generate is as follows.

1. Create an offset polyline $P'_0P'_1P'_2\dots P'_n$ by first creating the planar miter offset of $P_0P_1P_2\dots P_n$ by a constant width outward (left-side of the polyline) and moving the offset to the y direction. Specifically, to let ω and ϕ denote the width of each panel and the angle between the xz -plane and each panel, respectively, we choose the width of planar offset equal to $\omega \cos \phi$ and amount of translation in the y direction equal to $\omega \sin \phi$ in y . This particularly ensures parallelness of the edges of the original and offset polyline $P_iP_{i+1} \parallel P'_iP'_{i+1}$.
2. Similarly, create an offset polyline $P''_0P''_1P''_2\dots P''_n$ by first creating the planar miter offset of $P'_0P'_1P'_2\dots P'_n$ by $\omega' \cos \phi$ width inward (right side of the polyline) and moving the offset by $\omega' \sin \phi$ toward the y direction. In **fig. 14**, we selected $\omega = \omega'$.
3. Repeat Steps 1 and 2 as required.
4. Span quad panels between adjacent polylines.

The resulting structure is composed of degree-4 vertices where four sector angles are the same and thus transforms from the generated state to the completely flat-folded state, wherein everything lies on the xz -plane. Every folded state belongs to the same family generated from the abovementioned operation with different ϕ and polyline $P_0(\phi), P_1(\phi), \dots, P_n(\phi)$, where the polyline is represented as a function of ϕ . The polyline in the folded state can be computed from the isometry of each trapezoidal panel. Let θ_i denote the half exterior angle of polyline at $P_i(\phi)$; subsequently, because the length of offset polyline edge $P'_i P'_{i+1}$ stay constant, we obtain $\omega \cos \phi \tan \theta = \text{const.}$. Therefore, we obtain

$$\tan \theta_i = \sec \phi \tan \theta_i|_{\phi=0},$$

where $\theta_i|_{\phi=0}$ is the half exterior angle of the polyline at P_i when completely flat-folded. This particularly illustrates that the exterior angle of the polyline corners increase as it unfolds and becomes 180° when in its unfolded limit, when often the structures self-intersect. If the polyline $P_0 P_1 P_2 \dots$ is properly corrugated, obtaining structures that completely fold in two directions (**fig. 15** Right) without self-intersection is also possible.

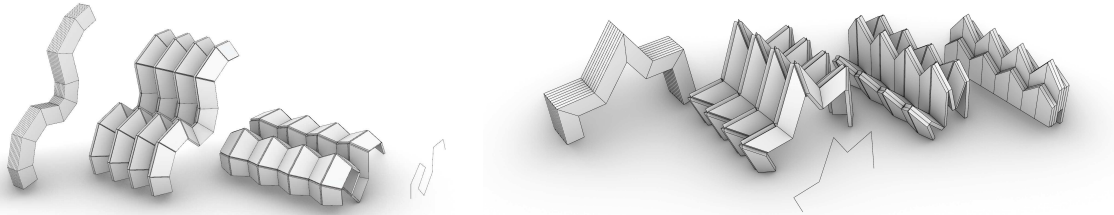


Figure 15: Left: One-way flat-foldable mechanism generated from a non-convex polyline wherein mountain and valley creases are alternately repeated only in one direction. Right: Bidirectionally flat-foldable mechanism generated from a zigzagged polyline wherein mountain and valley creases are alternately repeated in both directions.

The overall structure can be constructed with panels of a single thickness t because the four sector angles of every vertex are equal. Due to the shifted axes at the saddle-like vertices, we obtain an additional shift of panels by $2t \cos \phi$ towards the y direction at each valley corrugation. Moreover, at non-convex points on the polyline, the offset axes creates a shift in the xz plane, as shown in **fig. 14** middle row right. The structure with thickness can be flatly folded in the y direction, keeping every panel parallel to xz -plane, when the total thickness in y direction is the sum of thicknesses of the overlapping panels (**fig. 16**).

In **fig. 14**, we selected $\omega = \omega' = \omega'' \dots$ as this creates a compact flat-folded state, but we may choose a different width for each offset so that we may obtain doubly curved surfaces as in **fig. 17** with varying heights and width.

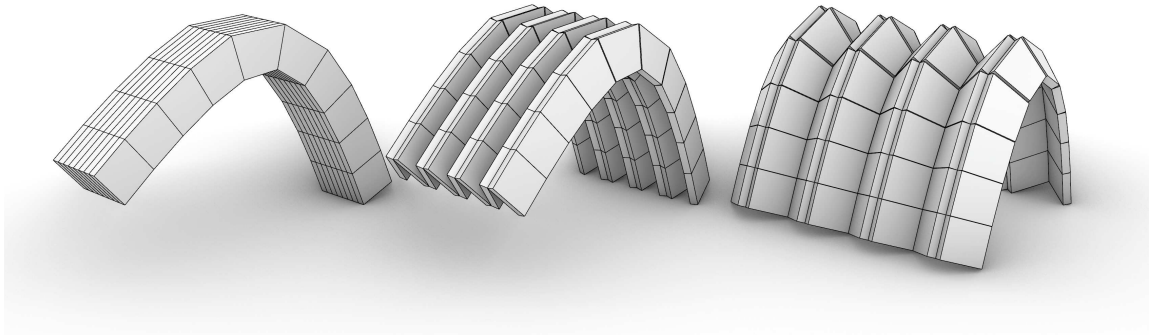


Figure 16: Flat-foldable parabolic vault wherein mountain and valley creases are alternately repeated only in one direction. Every panel has the same thickness.

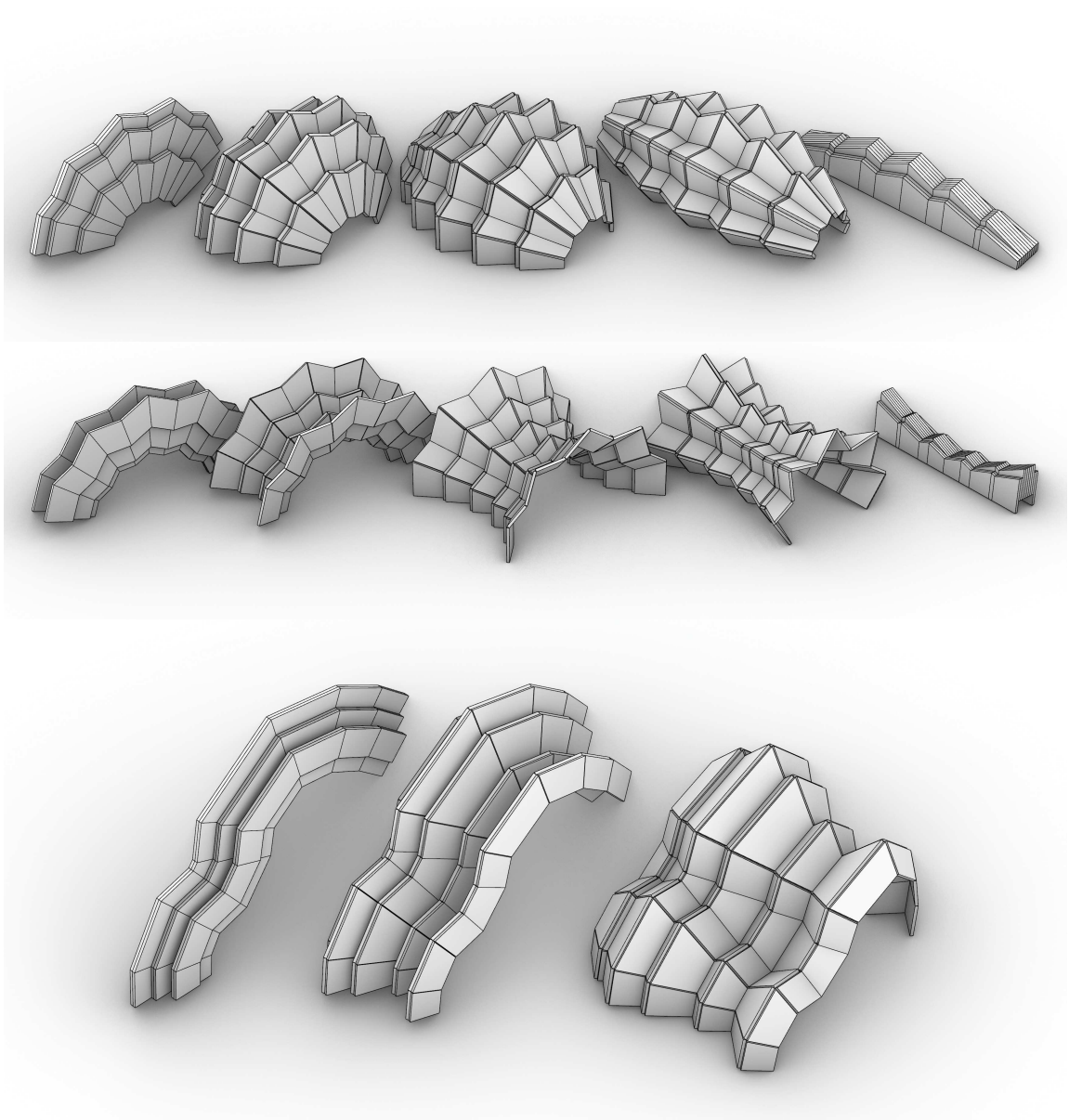


Figure 17: Doubly curved surfaces with varying heights and widths.

5.2 Bidirectionally Flat-Foldable Dome

Figure 18 shows a bidirectionally flat-foldable dome with 6×6 panels using the mirror symmetry about two perpendicular planes (**fig. 19** Right). The parameters are computed by solving the constraints for each quadrant composed of 3×3 panels, with constraints that the boundary must lie on the mirror planes. At each vertex on the mirror planes, the opposite and mirrored angles should be equal, i.e., all sector angles should be equal. Therefore, when a saddle-like vertex is on the mirror plane, all thicknesses of the panels connected to the vertex should be equal according to **eq. (5)** and **eq. (6)**. Considering the thickness arrangement that can satisfy this condition, two types of thicknesses can be applied, as shown in **fig. 19** left. Each quadrant has 25 sector angles of interior vertices, 8 pairs of opposite angles, 4 pairs of sector angles at the vertices on the mirror plane, 4 interior faces, 2 saddle-like vertices not on the mirror plane, and 2 thicknesses. Therefore, the DOF of design is $25 - 8 - 4 - 4 \times 2 - 2 + 1 = 4$.

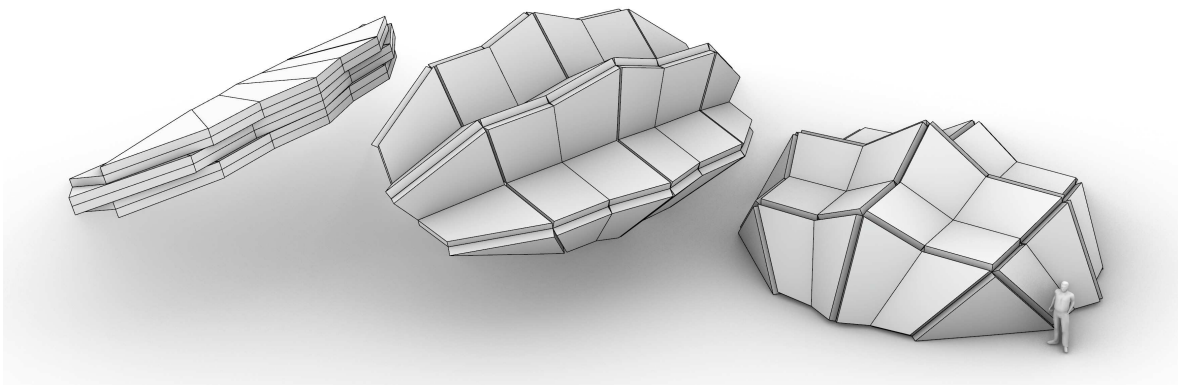


Figure 18: Generalized eggbox pattern wherein mountain and valley creases are alternately repeated in both directions. There are two types of thicknesses applied to the panels. Thickness a : 200mm, b : 210mm

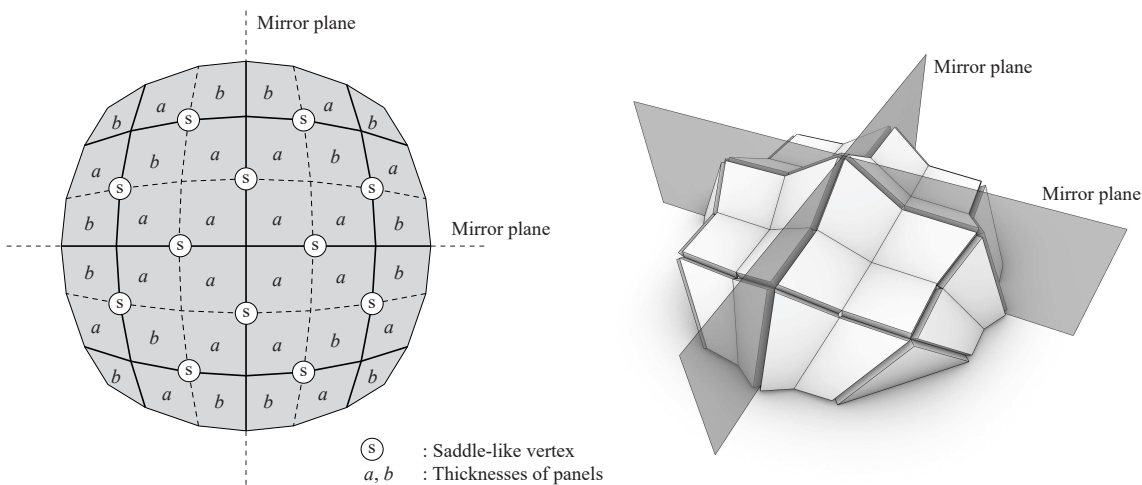


Figure 19: Left: the arrangement of panel thicknesses and saddle-like vertices. Right: the mirror planes of the flat-foldable dome.



Figure 20: Folding motion of the bidirectional flat-foldable model. Thickness a: 7mm, b: 8mm (assumed that standard dimensions of 21-mm and 24-mm thickness is used.)

6 Outlook and Future Works

Our method has an advantage for architectural fabrication. Because each panel has a constant thickness, it can be produced by only cutting out the panels of standard dimensions using a two-axis machine (e.g., a two-axis CNC router or a laser cutter) (**fig. 21** Top). The property that the structures folds completely flat with stacked panels is also useful for the assembly of panels. This property holds even when several thicknesses of panels are in use; they still are tightly stacked without interference or gaps between them. In the assembly process, we can stack the panels in its flat-folded state and attach hinges between the stacked panels from the exposed sides of panels.

Such a prefabrication process does not require scaffolding and is also potentially fully automated. We may extend our idea to interpret each thick panel to be a non-monolithic one; for example, we may prefabricate composite panels wherein structural elements, cladding, insulation, and facilities are already contained. Once we obtain the flat-folded shape with every architectural component prefabricated, we can transport it to the building site and deploy it for use (**fig. 21** Middle Bottom). After its use, the structure can be completely folded again and stored for later reuse.

In order to materialize the proposed structures, detailed structural design of hinges and panels during the deployment and under the static and dynamic loads after deployment are necessary; this is one of the future works of this work. Also, the family of surfaces are limited due to geometric constraints of discrete Voss surfaces and the thickness conditions. We would like to explore other design families of non-developable surfaces with thick panels in future.

Acknowledgement

This work is supported by JSPS KAKENHI 16H06106 and JST PRESTO JP-MJPR1927.

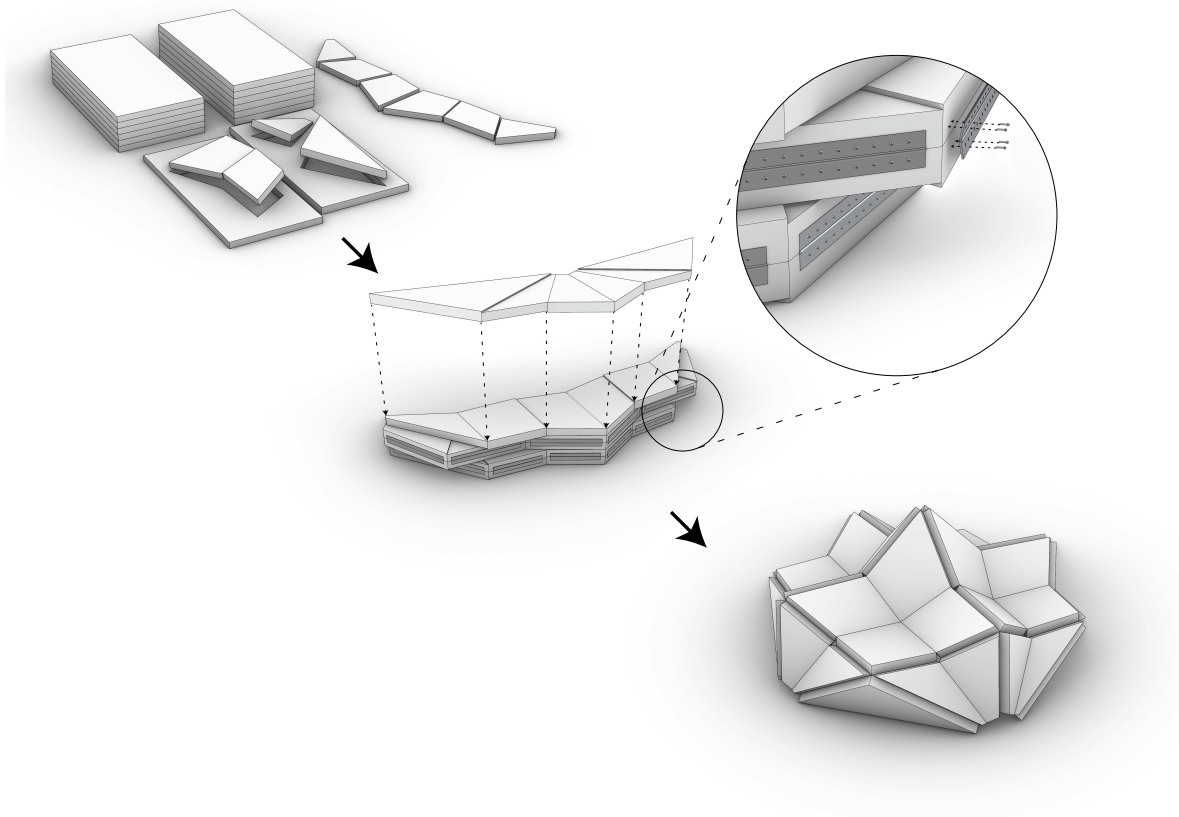


Figure 21: Top: each panel can only be cut out of standard material and therefore only be manufactured using a two-axis CNC. Middle: easy to assemble by simply piling them up and attaching hinges to end sections of panels. Bottom: the project will be completed by deploying it.

References

- Bennett, G. T. (1903). A new mechanism. *Engineering* 76, 777.
- Chen, Y., R. Peng, and Z. You (2015). Origami of thick panels. *Science* 349(6246), 396–400.
- Hoberman, C. (2010, September 14). Folding structures made of thick hinged sheets. US Patent 7,794,019.
- Hoberman, C. S. (1988, October 25). Reversibly expandable three-dimensional structure. US Patent 4,780,344.
- Lang, R. J., K. A. Tolman, E. B. Crampton, S. P. Magleby, and L. L. Howell (2018). A review of thickness-accommodation techniques in origami-inspired engineering. *Applied Mechanics Reviews* 70(1).
- Schief, W. K., A. I. Bobenko, and T. Hoffmann (2008). On the integrability of infinitesimal and finite deformations of polyhedral surfaces. In *Discrete differential*

geometry, pp. 67–93. Springer.

Tachi, T. (2010). Freeform rigid-foldable structure using bidirectionally flat-foldable planar quadrilateral mesh. *Advances in architectural geometry* 14(2), 203–215.

Tachi, T. (2011). Rigid-foldable thick origami. *Origami* 5, 253–264.

Tachi, T. and T. C. Hull (2017, 03). Self-Foldability of Rigid Origami. *Journal of Mechanisms and Robotics* 9(2). 021008.